JGR Space Physics

METHOD
10.1029/2022JA031061

Key Points:

- We present a new open-source tool for geomagnetospheric computations, named "Oulu—Open-source geomagneToSphere prOpagation tool" (OTSO)
- The new tool shows a good agreement with other tools that preform a similar function (e.g., MAGNETOCOSMICS)
- Ground level enhancement (GLE) 66 and 71 were both successfully analyzed using the tool proving that it can preform comprehensive GLE analyses for future studies

Correspondence to:

N. Larsen,
nicholas.larsen@oulu.fi;
nlarsen1505@gmail.com

Citation:

Larsen, N., Mishev, A., & Usoskin, I. (2023). A new open-source geomagnetosphere propagation tool (OTSO) and its applications. *Journal of Geophysical Research: Space Physics*, *128*, e2022JA031061. https://doi.org/10.1029/2022JA031061

Received 4 OCT 2022
Accepted 6 FEB 2023

Author Contributions:

Conceptualization: Nicholas Larsen
Formal analysis: Nicholas Larsen, Alexander Mishev
Funding acquisition: Nicholas Larsen, Alexander Mishev
Investigation: Nicholas Larsen, Alexander Mishev
Methodology: Nicholas Larsen
Project Administration: Alexander Mishev
Software: Nicholas Larsen
Supervision: Alexander Mishev, Ilya Usoskin
Visualization: Nicholas Larsen
Writing – original draft: Nicholas Larsen, Alexander Mishev
Writing – review & editing: Nicholas Larsen, Alexander Mishev, Ilya Usoskin

A New Open-Source Geomagnetosphere Propagation Tool (OTSO) and Its Applications

Nicholas Larsen[1,2], Alexander Mishev[1,2], and Ilya Usoskin[1,2]

[1]Sodankylä Geophysical Observatory, University of Oulu, Oulu, Finland, [2]Space Physics and Astronomy Research Unit, University of Oulu, Oulu, Finland

Abstract We present a new open-source tool for magnetospheric computations, that is modeling of cosmic ray (CR) propagation in the geomagnetosphere, named "Oulu—Open-source geomagneToSphere prOpagation tool" (OTSO), available on GitHub (https://github.com/NLarsen15/OTSO) and Zenodo (https://doi.org/10.5281/zenodo.7516233). A tool of this nature is required in order to interpret experiments and study phenomena within the CR research field. Within this work, OTSO is applied to the investigation of several ground-level enhancement events. Here, we demonstrated several applications of OTSO, namely the computation of asymptotic directions of selected CR stations, effective rigidity cut-off across the globe at various conditions within the design, and general properties, including the magnetospheric models employed. Comparison and validation of OTSO with older widely used tools such as MAGNETOCOSMICS was performed, and good agreement was achieved. An application of OTSO for providing the necessary background for the analysis of two notable ground-level enhancements is demonstrated and their spectral and angular characteristics are presented.

Plain Language Summary Cosmic rays (CRs) are hazardous to humans and are constantly bombarding the Earth. Some impacts of these CRs are increased radiation doses for aviation crew and their passengers and damaging spacecraft. Luckily the Earth's magnetic field deflects most of these harmful particles away, mitigating most of the potential damage. The interaction between the Earth's magnetic field and incoming CRs is complex but needs to be properly understood and accurately modeled for the study of specific phenomena relevant to the CR research field. This work presents a new open-source tool for magnetospheric computations named the "Oulu—Open-source geomagneToSphere prOpagation tool" (OTSO). This tool can compute the trajectory of CRs within the Earth's magnetic field under various magnetospheric conditions. Within this work, comparison and validation of OTSO with an older widely used tool (MAGNETOCOSMICS) was performed with a good agreement observed. OTSO was also used to successfully aid in the analysis of two ground-level enhancement events. OTSO demonstrates its usefulness as a tool to aid in the study of CRs in the magnetosphere, and its open-source nature allows for further development by the research community.

1. Introduction

The Earth is under constant bombardment by high-energy particles known as cosmic rays (CRs). Primary CRs can have a solar, galactic or extra-galactic origin and are composed of ≈90% protons, 9% helium nuclei, and 1% heavier element nuclei (e.g., Gaisser et al., 2016, and references therein). CRs with a solar origin, also known as solar energetic particles (SEPs), are produced during and following solar eruptions, such as solar flares and/or coronal mass ejections (e.g., Desai & Giacalone, 2016, and references therein), whilst CRs produced outside of the solar system are believed to come primarily from supernova remnants (e.g., Blasi, 2013, and references therein). CRs were first discovered in the early 20th century by Dr. Victor Hess and since then our knowledge of CRs has been constantly developing through the application of ground-breaking experiments, recent examples include the Payload for Antimatter Exploration and Light-nuclei Astrophysics (PAMELA) detector (Adriani et al., 2017), AMS-02 (Alpha Magnetic Spectrometer) (Aguilar et al., 2021) space-probes, and a plethora of ground-based experiments.

If a CR reaches the Earth's atmosphere it collides with atmospheric constituents. This collision produces numerous secondary particles, which then proceeds to collide or decay further into more secondary particles creating a cascade, the process developing until a threshold energy is reached. This phenomenon is known as an extensive air shower and is widely exploited by ground-based detectors as a mechanism for study CRs. Within this work

neutron monitors (NMs) are used as an example for CR detection, specifically of solar origin. NMs are fixed to a single location on the Earth making them especially good at studying CRs of solar origin, typically revealing anisotropy (e.g., Bütikofer et al., 2009; Moraal & McCracken, 2012). When NMs detect an increased flux of CRs with solar origin, it is dubbed a ground level enhancement (GLE), a relatively rare event that occurs only a few times per solar cycle (Shea & Smart, 2012). Introduced during the 1957–1958 International Geophysical Year, NMs are standardized, nowadays assembled in a global network (Mavromichalaki et al., 2011; Simpson, 2000).

CRs are charged particles and as such experience the Lorentz force when traveling within a magnetic field. Thus, when a CR encounters the Earth's magnetic field there is the potential for the CR to be deflected by the magnetic field or penetrate it. The ability of the Earth's magnetic field to deflect certain CRs is known as magnetic shielding. Whether a CR is able to penetrate the magnetosphere depends greatly on its energy, the geomagnetic conditions at the time of arrival, the location of the CR's arrival, and its incidence. Only once a CR has penetrated the magnetosphere can it proceed to reach the Earth's atmosphere. An important characteristic of CRs is their rigidity, this value is typically used instead of CR energy as it is independent of the CR charge and species (Cooke et al., 1991). Rigidity quantifies the impact that magnetic fields have on the propagation of the CR, the larger the rigidity value the less deflected the particle is by a magnetic field. The rigidity of a CR is calculated using equation:

$$P = \frac{pc}{Ze} \tag{1}$$

where P is the rigidity, p is the CR's momentum, c is the speed of light, Z is the atomic number, and e is the elemental charge. Rigidity is important when considering CRs arriving at Earth as it can tell us which CRs are able to penetrate the magnetosphere and which are deflected away as a result of magnetic shielding. The rigidity needed by the CR to penetrate the magnetosphere ranges from 0 GV, at the magnetic poles, to ≈17 GV at the magnetic equator, this is due to the increase in magnetic shielding at lower latitudes (Gerontidou et al., 2021). Knowing the rigidity needed by a CR to arrive at different locations on the Earth (known as the cutoff rigidity) is important to analyze both ground-based and inside the geomagnetosphere space-borne experiments.

Determining an exact cutoff rigidity can be a difficult task due to the complex nature of CR propagation in the magnetosphere. It is typical to see a collection of CRs with sequential rigidities having a mixture of trajectories that can and cannot penetrate the magnetosphere, referred to allowed and forbidden respectively (for details see Cooke et al., 1991). This region of allowed and forbidden CR trajectories is known as the penumbra. In order to get a useful quantitative value for the cutoff at given points on the Earth's surface an effective cutoff rigidity (R_c) is found, which accounts for the effects of the penumbra. As mentioned previously, the trajectories of CRs can be very complex, increasingly so at lower rigidities, this means that CRs that are detected, at for example NMs, do not necessarily arrive from directly above the station, therefore each station has its own asymptotic direction (AD) of acceptance for CRs, that is which part of the sky the detector is actually observing (Rao et al., 1963).

The complex nature of the Earth's magnetic field structure and CR propagation within it makes modeling CR trajectories very computationally intensive. The equations of motion that describe the trajectory of a charged particle in the Earth's magnetosphere currently have no known closed form solution. As such the trajectory of said particle must be determined using numerical integration (e.g., Bütikofer, 2018). It is almost impossible to predict where an arriving CR will encounter the Earth based on its point of arrival at the magnetosphere, therefore, the trajectory is typically computed backwards from just above the Earth's surface, around 20 km in altitude, to the CR's point of entry into the magnetosphere.

During GLEs, SEPs can have energies ranging from 10 MeV/nucleon up to about several GeV/nucleon (Biswas, 2000), relativistic effects should thus be accounted for in the model. To resolve any issues that can arise from this, the computation of the particle's trajectory must be done in small steps to avoid the model breaking, however this exacerbates the computational intensity of the modeling process. Finding a good balance between maintaining accuracy of the simulation and time efficiency is one of the main tasks of creating a magnetosphere computation tool.

The magnetosphere is a complex and dynamic environment, constantly changing in response to external conditions, which makes the accurate modeling very challenging. Empirical observations made by spacecraft have been used historically to create models describing the magnetic field structure (Jordan, 1994). As of present the field is best described as a combination of the inner magnetic field (created by the dynamo process in the Earth's

core) and external magnetic fields (created by the various different currents within the magnetosphere). For the internal field, models such as the international geomagnetic reference field (IGRF) (Alken et al., 2021) and dipole models (Nevalainen et al., 2013) can be used and for external fields the Tsyganenko models are typically used (Tsyganenko, 1989, 1995, 1996, 2002a, 2002b).

A tool that can compute the trajectories of charged particles within an accurate model of the magnetosphere under various conditions is highly valuable within the CR research field. The usefulness of such a tool has led to the creation of multiple tools in the past (see Bütikofer, 2018 and references therein), some examples are the tool developed by D. F. Smart and Shea (2001), Cut-off rigidity model (COR) by Gecášek et al. (2022), and MAGNETOCOSMICS by Desorgher (2006), the latter taken as a reference tool in this work, being widely used over the years. We emphasize that MAGNETOCOSMICS was designed within the framework of the Geant4 toolkit (Agostinelli et al., 2003), was released in 2006, and is in practice outdated nowadays. The only way to resolve this issue is to either update MAGNETOCOSMICS to be compatible with the newer Geant4 versions or create a new tool. Here we have chosen the latter approach and present the newly developed Oulu—Open-source geomagneToSphere prOpagation tool (OTSO), which can be tailored by the scientific community to meet the corresponding needs. OTSO is a downloadable tool that the user will be able to access from their computer and freely edit.

2. Oulu—Open-Source GeomagneToSphere PrOpagation Tool (OTSO)

2.1. Formalism of CR Propagation

The trajectories of charged particles are influenced by the magnetic field generated by the Earth's core. This is due to the Lorentz force generated perpendicular to a charged particle moving through a magnetic field. The Lorentz force is described by:

$$\mathbf{F} = q\mathbf{E} + q(\mathbf{v} \times \mathbf{B}) \tag{2}$$

where $\mathbf{F}$ is the force $[N]$, q is the charge $[C]$, $\mathbf{E}$ and $\mathbf{B}$ are the electric $[\mathrm{V\,m^{-1}}]$ and magnetic fields $[T]$ respectively, and $\mathbf{v}$ is the particle's velocity $[\mathrm{ms^{-1}}]$.

When considering magnetosphere calculations we can neglect $\mathbf{E}$ from the equation as its influence is negligible due to the high electrical conductivity of the region (for details see Bütikofer (2018) and the discussion therein). It is important to note that the bulk of CRs are traveling at relativistic speeds and as such the impact this has on the particle's mass must be considered when calculating the acceleration. This is achieved by incorporating the Lorentz factor γ:

$$\gamma = \sqrt{\frac{1}{1 - \left(\frac{v}{c}\right)^2}} \tag{3}$$

Combining Equation 2 and the Lorentz factor within Newton's second law we can determine the equations of motion for a relativistic particle as a result of the Lorentz force within the magnetosphere in Cartesian coordinates:

$$\begin{aligned}
\frac{dx}{dt} &= v_x \\
\frac{dy}{dt} &= v_y \\
\frac{dz}{dt} &= v_z \\
\frac{d^2x}{dt^2} &= \frac{q}{\gamma m_0}\left(B_z\frac{dy}{dt} - B_y\frac{dz}{dt}\right) \\
\frac{d^2y}{dt^2} &= \frac{q}{\gamma m_0}\left(B_x\frac{dz}{dt} - B_z\frac{dx}{dt}\right) \\
\frac{d^2z}{dt^2} &= \frac{q}{\gamma m_0}\left(B_y\frac{dx}{dt} - B_x\frac{dy}{dt}\right)
\end{aligned} \tag{4}$$

with m_0 being the rest mass of the particle. Knowing the acceleration of the CR at a specific point in the magnetosphere allows for the trajectory to be determined by performing numerical integration of the equations of motion,

as there is no solution in their enclosed form. There are multiple methods that can be implemented to achieve this, such as the Runge-Kutta, Euler, Boris, and Vay methods. All of these methods have their own benefits and drawbacks when considering computation speed and accuracy (see Costa Jr. and Leigui de Oliveira 2019 and references therein). The most widely used method in CR simulations is the 4th order Runge-Kutta method discussed by D. F. Smart et al. (2000), and as such it has been incorporated into the present work. This method offers a good balance between approximation accuracy and calculation time. Other integration methods can be added to OTSO later if required.

The trajectory of the particle is then determined up until the allowed or forbidden condition for the trajectory is met. Similarly to D. F. Smart and Shea (1981), we employ the approach of starting the particle propagation at 20 km above the surface, this start value can be changed within OTSO by the user, with the particle's velocity being directed vertically at the zenith. While a vertical zenith is typically adopted for GLE analysis, for study of strong or very anisotropic events the obliquely incident particles are also important and can be accordingly considered (see Clem, 1997; Cramp et al., 1997), therefore, OTSO provides the option of altering the azimuth and zenith angles to meet the users needs. This is an important step in increasing the robustness of the tool as the trajectories of incoming particles are significantly influenced by the direction of arrival in addition to their rigidity. With the inclusion of user defined zenith and azimuth parameters the applications of OTSO expand beyond just GLE analysis (e.g., investigations into East-West asymmetry and calculating non-vertical effective cutoff rigidities). The trajectory is considered allowed if the particle is then able to reach the model magnetopause boundary and forbidden if it returns below the 20 km starting altitude. We emphasize that 20 km is selected as this is the typical altitude that atmospheric cascades start as a result of CR collisions with atmospheric particulates (Grieder, 2001). While collisions are possible above this point the model assumes the atmosphere is collisionless until 20 km for simplicity. In addition, the tool ends the simulation once the CR has traveled more that 100 Earth radii, to avoid endless simulation of a trapped particle that neither escapes or returns to Earth, and in this instance the trajectory is assumed forbidden. Both the minimum altitude and maximum distance traveled for the modeling can be parameterized by the user, 20 km and 100Re have been selected respectively within this work as sensible base values.

OTSO can calculate individual trajectories of CRs with any given initial rigidity and start position on the Earth's surface. The user can select a range of rigidity values to test across as well as a rigidity step value, ΔR. OTSO will then repeat the trajectory calculation over all iterations of rigidity within the given range determining allowed and forbidden rigidity values. Due to the penumbra, that is encountered around the region in which rigidities change from allowed to forbidden, it is important to know the upper most accepted rigidity before the first forbidden value, R_U, and the last allowed value, R_L. These values are recorded during computations and to account for the effect of the penumbra an effective cutoff rigidity, R_c, is calculated using a method described in Cooke et al. (1991). In which the sum of the number of allowed rigidities multiplied by ΔR is subtracted from R_U, seen in Equation 5.

$$R_c = R_U - \int_{R_U}^{R_L} \Delta R_{(allowed)} \tag{5}$$

2.2. Determining Time-Step

One of the most important parts of the computation is determining the time-step (Δt) to use during the numerical integration of the equations of motion. If Δt is too large then errors will accumulate leading to incorrect trajectories or the simulated particles accelerating to speeds faster than light, breaking the simulation. Vice versa, if Δt is too small then the computation can take an irrationally long time to complete, making the tool impractical to use.

A convenient way to determine Δt involves using the CR's properties and position in the magnetosphere. This work uses the method developed within D. F. Smart and Shea (1981) in which Δt is the time taken for the particle to travel 1.0% of its gyration distance, making the assumption the magnetic field is uniform over the step. In order to optimize the computation further, the adaptive time-step method also outlined within D. F. Smart and Shea (1981) was utilized. This allows Δt to grow by a maximum of 10% between Runge-Kutta iterations, only if the previous iteration was completed within an accepted error range, and sets the maximum value of Δt to be 1.5% of the gyration time. This growth limit prevents any regions of sudden acceleration being skipped by large

Δt values. However, through testing of the new program the 1.5% limit was found to lead to extended computation times and was changed to 15% with marginal impact on the results of the calculations. This limit can be edited or disabled depending on the accuracy of results required by the user and the desired computation time. The error between Runge-Kutta iterations is determined by checking the β value of the CR before and after the step, where β is the speed of the CR in units of c. As a charged particle in a magnetic field, with no other external force, should have a constant speed we can take the change in β to represent the error between steps. Within the tool this is implemented so that if β has grown by over 0.0001% during a Runge-Kutta step Δt is assumed too large and the same iteration is repeated using $\frac{\Delta t}{2}$. This β error check is quite conservative and reduced error values have been able to reproduce similar results in a vastly reduced computation time, especially at higher latitude stations. The value of this error check parameter can be selected at the leisure of the user.

2.3. Employed Magnetosphere Models

In order to model the magnetic field OTSO uses an internal and external magnetic field model. There are only two main internal field models included in OTSO, these being the IGRF (Alken et al., 2021) and geodipole field models. Presently the user can choose to model the external component of the magnetic field using the any of the following Tsyganenko models: TSY87, TSY89, TSY96, TSY01, and TSY01S (Tsyganenko, 1987, 1989, 1995, 1996, 2002a, 2002b, 2003). We plan to include other models in the future, based on a convenient parameterization. This allows for easier comparison with, for example, MAGNETOCOSMICS and/or other similar tools. The latter Tsyganenko models get increasingly complex and computationally intensive, leading to long simulation times. The use of later Tsyganenko models should be considered during periods of intense geomagnetic activity (e.g., periods of Kp index above 6). Generally a combination of the IGRF and TSY89 models is sufficient to provide fast and reliable results (e.g., Kudela & Usoskin, 2004; Nevalainen et al., 2013, and the discussion therein). As such, this combination of models is taken as a good default for OTSO and the computations in this paper are conducted using said combination. TSY01 is also used for the analysis of GLE #66 in subsection 3.3 to investigate the differences between the two external models for an extreme event occurred during exceptionally strong geomagnetic disturbance. Unless stated differently, the future calculations using OTSO will be performed using this combination of models.

In order to determine whether a CR has escaped the magnetosphere, this tool constantly checks the CR's position in relation to the model magnetopause chosen for the simulation. If the CR reaches the magnetopause boundary it is then assumed to have escaped. The TSY96, TSY01, and TSY01S models for the external magnetic field contribution use their own model magnetopause described within Tsyganenko (1995, 1996, 2002a, 2002b). However, TSY89 has no such empirical magnetopause model used within it and therefore a “de-facto” boundary must be selected by the user which is then applied to the simulation when using the TSY89 model.

Models of the magnetopause have historically been produced using empirical methods, utilizing data from satellite magnetopause crossings to best fit the shape. The models that have been included in the tool currently are a sphere with a radius of 25 Earth radii centered around the Earth (for use when not considering any external field models) as well as the Formisano, Sibeck, and Kobel models (Flückiger & Kobel, 1990; Formisano et al., 1979; Kobel, 1992; Sibeck et al., 1991). Due to the differing assumptions made during the creation of these models the magnetopause shape can vary significantly between them, leading to slightly different simulation outcomes. When using TSY89 within this work the Kobel (1992) model has been used.

There are many more advanced magnetopause models that take into account different variables, such as the solar wind conditions. Some examples of newer models are Lin et al. (2010) and Shue et al. (1998). While these models may provide a more accurate portrayal of the magnetopause they are not included in this tool at present. These models require many more input variables to function, complicating and increasing the computational strain of the simulation. Their inclusion is planned to be accommodated in future versions of the tool if the need arises for the extra accuracy they may provide.

2.4. Programming Languages

OTSO has been developed within the framework of both the python and fortran programming languages. A precompiled language, such as fortran, was crucial in the development of this tool as the processing speed offered by compiled languages help complete the computationally intensive CR trajectory simulations within

Table 1
Data for the Calculated Effective Vertical Cutoff Rigidity for Selected Neutron Monitors Using Both OTSO and MAGNETOCOSMICS

	Vertical cutoff rigidity (GV)	
Station	MAGNETOCOSMICS	OTSO
Apatity	0.516	0.527
Calgary	0.92	0.924
Cape Schmidt	0.368	0.377
Fort Smith	0.158	0.167
Kerguelen	0.933	0.947
Kingston	1.725	1.738
Lomnický štít	3.633	3.644
McMurdo	0.000	0.000
Oulu	0.622	0.647
Rome	6.091	6.089
Terre Adelie	0.000	0.000
Tixie Bay	0.416	0.441

Note. A visual comparison between the two tools can be seen in Appendix A.

a reasonable time frame. Fortran is an old and dated language, with limited utility when compared to other more modern complied languages, such as C++. However, fortran does benefit from being an older language by being relatively simple as well as having many freely accessible and verified libraries previously written for it, which are already extensively used by the CR community, such as the Tsyganenko models, geopack library, and IRBEM library (https://prbem.github.io/IRBEM/). For these reasons fortran was chosen to utilize these libraries and speed up the development of this tool.

Python was also used as the way to initialize the tool and input the parameters. Python is a very simple programming language and was picked to allow anyone with a basic understanding of programming to use the tool. The installation of the python language is also simple, being easily achieved through the download of the anaconda software. Anaconda also includes all the needed python modules needed for the tool to run, such as F2PY (which allows python and fortran to transfer information between each other).

The result of both these decisions is that the tool is simple to obtain, use, and edit.

3. Example Results, Comparison, and Applications

As this tool is being constructed to be a possible alternative to older programs, namely MAGNETOCOSMICS, the analysis of this new tool relies on the comparison of results between the two programs. To achieve this, several cases were selected, specifically related to GLE analysis, and both programs were used to conduct computations for said GLE(s). The first case is a well-studied, within not complicated as magnetospheric conditions, derived characteristics GLE event, namely GLE # 70 (Bütikofer et al., 2009; Mishev & Usoskin, 2016; Vashenyuk et al., 2006).

3.1. GLE 70

GLE # 70 occurred on 13 December 2006 during the declining phase of solar cycle 23 as the result of a X3.4/4 B solar flare, with an associated GLE being detected around 03:00 UTC. The Tsyganenko (1989) model uses an integer parameter known as IOPT as a convenient way to parameterize the geomagnetic field distortion at the desired time of modeling. The value of IOPT ranges between 1 and 7 depending on the Kp index, the higher the IOPT value the greater the geomagnetic distortion. The value of IOPT is given as the Kp index plus 1, however at Kp values above 6 the IOPT value is always set to 7. For GLE # 70 the IOPT was set to 5, this corresponds to a planetary Kp index value of 4−, 4, 4+ at the time of the GLE. 12 NM stations at various latitudes were used to test OTSO by conducting cutoff and asymptotic cones computations. All computations were done using a rigidity step of 1×10^{-3} GV, increasing the precision of the results and allowing the penumbra to be shown in greater detail, and employing combination of IGRF and TSY 89 models.

3.1.1. Cutoff Rigidity

The results for the vertical cutoff computations can be seen in Table 1, where a general good agreement between the OTSO and MAGNETOCOSMICS is found. The stations with the greatest difference between the two tools were Oulu and Tixie Bay. The slight variation in results can be attributed to the accuracy of the integration methods used within the two tools.

As mentioned in Section 1 there are multiple other tools that can perform the same computations as OTSO and MAGNETOCOSMICS, namely COR (Gecášek et al., 2022; D. Smart & Shea 2020). A good agreement is also seen between OTSO and these other tools. For posterity a comparison between all of these tools, Table A1, is included in the appendix.

3.1.2. Asymptotic Cones

Once the trajectory of a CR has been simulated the asymptotic longitude and latitude are computed. The CRs with accepted trajectories then have these values plotted in order to construct the asymptotic cone of acceptance.

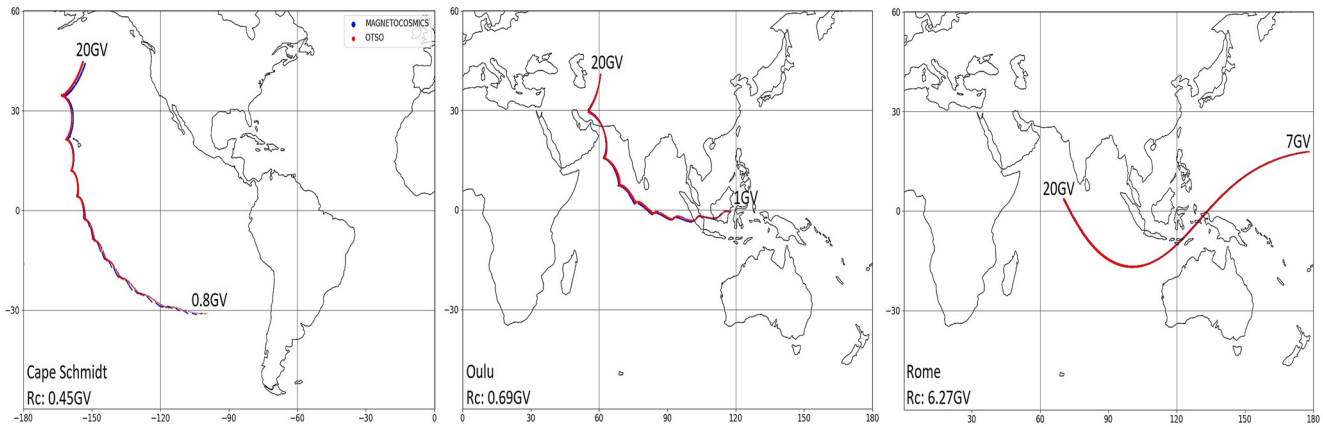

Figure 1. Computed asymptotic cones over various rigidity ranges for three selected neutron monitors (NMs) during GLE # 70 using both OTSO and MAGNETOCOSMICS, as denoted in the legend. The NMs, as well as their associated accepted R_c value, shown are: Cape Schmidt (left), Oulu (middle), and Rome (right).

Figure 1 shows the high rigidity value region of the cones created by OTSO and MAGNETOCOSMICS for three of the NM stations considered: Cape Schmidt, Oulu, and Rome respectively, encompassing the case of anti-sunward NM (CAPS), polar sunward (Oulu), and low latitude station (Rome).

One can see that the cones are in good agreement with each other, this is particularly true at the higher end of the rigidities. The cones calculated for the Oulu, and Rome NMs (see Figure 1) are almost identical with minor variations, however Cape Schmidt's cone shows that there can be some deviations in the cone shape between the two tools at lower rigidity values, namely the width of the OTSO cone increased (left panel of Figure 1). This is because the trajectories of lower rigidity CRs are more complex, especially when their rigidity is close to the cutoff value, making simulation of these CRs more difficult. The accuracy of the integration method is important in these circumstances and is likely the cause of the difference.

3.2. Global Cutoff

OTSO can compute the vertical cutoff rigidity on a global scale. Due to the mixed language nature of the tool multi-core processing was implemented using python to conduct the large number of computations required for this operation in a time efficient manner. The global cutoff map was created by conducting cutoff calculations at regular intervals of 1° in latitude and longitude. The same computation was done using MAGNETOCOSMICS and, in order to compare the two results, the absolute value for the difference between the computed cutoff rigidities at each point on the Earth was found and plotted in Figure 2. There are two clear results that can be inferred from Figure 2. First, in general the difference between the two tools is minor, this is especially evident in the polar and equatorial regions where the absolute difference is generally 0 GV. To further emphasize this point the relative difference between the two tools was computed (see Gecášek et al., 2022, and the discussion therein). For this comparison the locations with cutoff values of 0 GV were omitted as they would lead to disproportionately high relative differences when compared to the absolute difference in the region. The relative differences between −5% and 5%, a range selected to encompass regions with good agreement, are shown in Figure 3. Figure 3 clearly shows the good agreement around the magnetic equator as mentioned earlier. The mean and median relative differences were found to be −3.62% and 0.08% respectively, suggesting that OTSO and MAGNETOCOSMICS provide similar results, but OTSO generally tends to provide lower values for the effective vertical cutoff. Second, there are anomalous regions on the Earth where the difference between the two tools is noticeable, with the most prominent region being found over the south pacific ocean. The greatest cutoff difference of 1.31 GV is found in this south pacific region at a location of −37° latitude and −126° longitude, where OTSO and MAGNETOCOSMICS have an effective vertical cutoff of 7.92 and 9.23 GV respectively. Figure 4 looks into this anomalous region in more detail. Within Figure 4 OTSO shows a gradual decrease in rigidity values with a significant penumbra present across the south pacific anomaly. In contrast MAGNETOCOSMICS' plot is much more sporadic with sudden changes in R_u and R_l with a small penumbra is some regions, leading to the difference in R_c seen in Figure 2 within this region. Figures 2 and 3 show that, in general, both tools provide similar results, and that this is particularly true in the polar and equatorial regions. Figure A1 also supports this good agreement

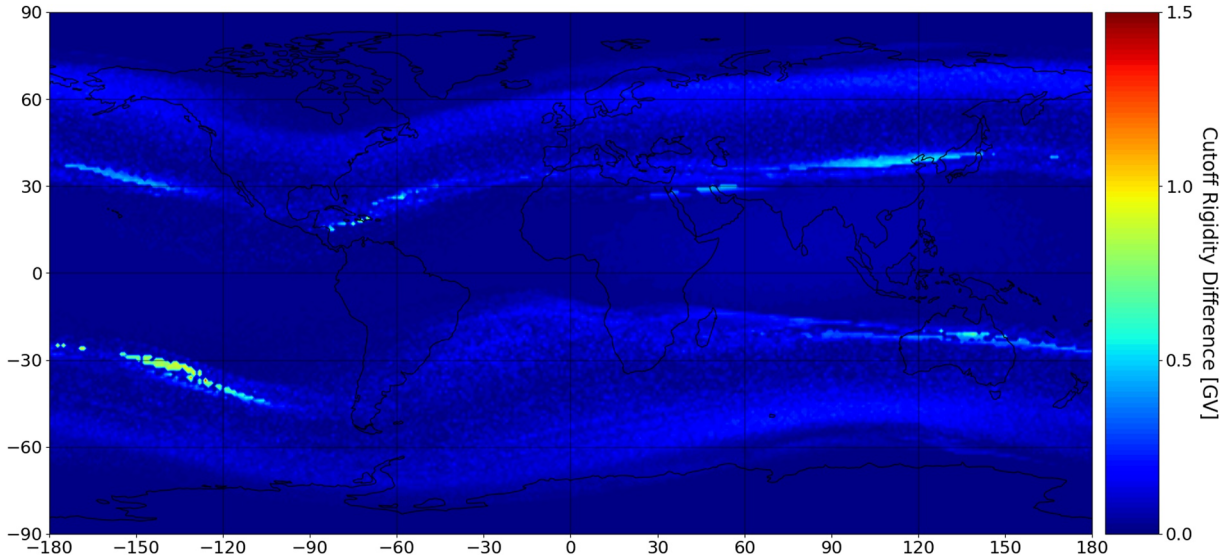

Figure 2. Absolute difference in calculated effective vertical cutoff rigidities for the entire Earth during GLE # 70 between OTSO and MAGNETOCOSMICS.

when looking at individual locations of NMs around the globe. The differences in tools are more pronounced in the mid latitude locations where CR propagation becomes more complex leading to intricate penumbras. In these regions the precision of the used integration method becomes more salient.

3.3. Ground Level Enhancement Analysis

OTSO was employed for GLE analysis, namely for computations of the cutoff rigidity and ADs for NMs used as input for the method deriving spectral and angular distribution of SEPs. Here, we used a method based on NM records analysis (e.g., Cramp et al., 1997; Shea & Smart 1982), whose details and applications are given elsewhere (Mishev, Koldobskiy, Usoskin, et al., 2021; Mishev et al., 2018, 2022). The method is an unfolding procedure, that is modeling the global NM network response and optimization of the model response over experimental data, which involves computation of the ADs and cutoff rigidity of NM stations used for the data analysis; assuming a convenient initial guess for the optimization (e.g., Cramp et al., 1995; Mishev et al., 2017); selection of model parameters and the optimization itself (Mishev & Usoskin, 2016). The method was recently verified by

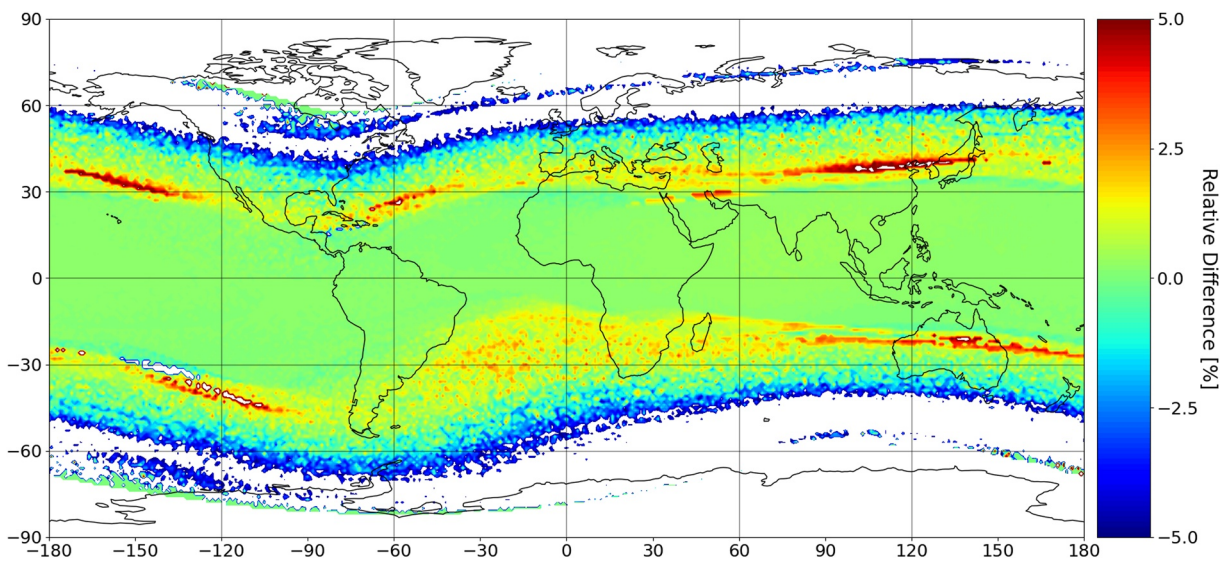

Figure 3. Relative differences in calculated effective vertical cutoff rigidities within the range of −5%–5% for the entire Earth during GLE # 70 between OTSO and MAGNETOCOSMICS.

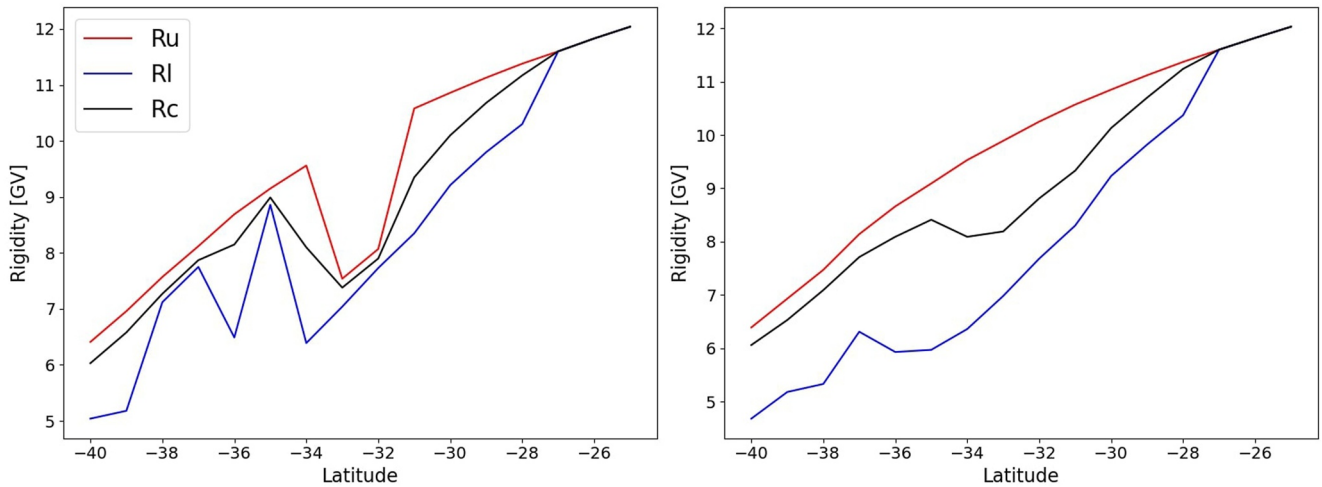

Figure 4. Cross sections of the cutoff rigidity values over the region of largest difference between MAGNETOCOSMICS (left) and OTSO (right), taken at a longitude of −140°.

direct space-borne measurements (for details see Koldobskiy et al., 2019, 2021; Mishev, Koldobskiy, Kocharov, & Usoskin 2021). The ADs were computed employing the aforementioned two field combination: internal, namely IGRF geomagnetic model (Alken et al., 2021), and external model, Tsyganenko 89 (Tsyganenko, 1989) or Tsyganenko 01 (Tsyganenko, 2002). The former combination allowed straightforward computation of ADs and rigidity cutoffs with reasonable precision (e.g., Kudela & Usoskin 2004; Kudela et al., 2008; Nevalainen et al., 2013), whilst the latter is usually employed in the case when the K_p index is greater than 6 (for details see D. F. Smart et al., 2000). For the unfolding we employed the method found within Levenberg (1944) and Marquardt (1963) with variable regularization by Aleksandrov (1971) and algorithm by Tikhonov et al. (1995) and Golub et al. (1999), which allowed reliable solution(s) to be obtained, even in the case of ill-posed problem(s) (Aster et al., 2005; Mavrodiev et al., 2004).

Here we analyzed two notable GLEs: GLE # 66 and GLE # 71. The GLE #66 occurred during one of strongest geomagnetic storms when the 3-hr planetary K_p index was 9, on 29 October 2003. The event was the second in the sequence of three GLEs, the so-called Halloween events (e.g., Gopalswamy et al., 2005; Gopalswamy et al., 2012; Liu & Hayashi 2006), recorded by the global NM network, the count rate increases are given in (http://gle.oulu.fi). In addition to the complicated geomagnetospheric conditions, a strong Forbush decrease, which is a period of decreased CR flux (for details see Forbush, 1937), was also observed prior to and during this event, which was explicitly considered in our analysis similarly to Mishev, Koldobskiy, Kocharov, and Usoskin (2021). Hence, the complicated geomagnetospheric conditions and accompanying Forbush decrease, make the analysis of this particular GLE specifically challenging. After computing the ADs with OTSO (see the left panel of Figure 5), and employing the method described above, we derived the spectral and angular characteristics of the GLE producing SEPs.

The best-fit of the derived SEP spectra was obtained by a modified power-law rigidity spectrum (e.g., Mishev, Koldobskiy, Kocharov, and Usoskin 2021; Vashenyuk et al., 2008), that is,

$$J_{\parallel}(P) = J_0 P^{-(\gamma+\delta\gamma(P-1))}, \tag{6}$$

where the flux of particles with rigidity P in [GV] is along the axis of symmetry identified by geographic latitude Ψ, longitude Λ and the power-law exponent is γ with the steepening of $\delta\gamma$, J_0 is the particle flux at 1 GV in $[m^{-2}\,s^{-1}\,sr^{-1}\,GV^{-1}]$, for SEPs with rigidity $P > 1$ GV. Accordingly, for SEPs with $P \leq 1$ GV, the rigidity spectrum is:

$$J_{\parallel}(P) = J_0 P^{-(\gamma+\delta\gamma\cdot P)}. \tag{7}$$

For the angular distribution the best-fit was obtained by Gaussian-like distribution:

$$G(\alpha(P)) \sim \exp\left(-\alpha^2/\sigma^2\right), \tag{8}$$

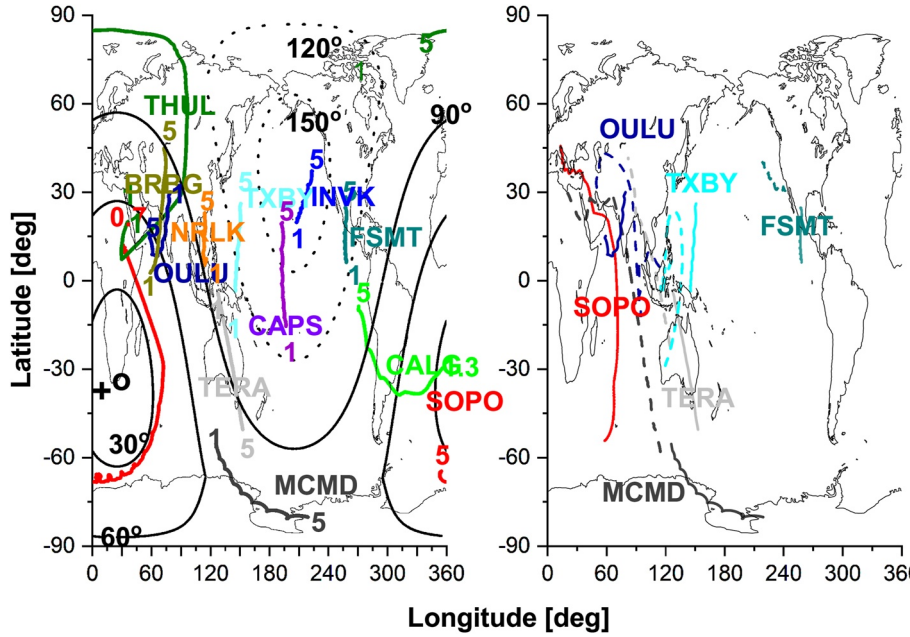

Figure 5. Left panel: asymptotic directions (ADs) (IGRF + TSY 89) of selected neutron monitor (NM) stations during GLE #66 at 21:00 UT. The small circle depicts the derived apparent source position, and the cross the interplanetary magnetic field direction obtained by the Advanced Composition Explorer satellite. The lines of equal pitch angles relative to the derived anisotropy axis are plotted for 30°, 60°, and 90° for sunward directions, and 120°, 150° for anti-Sun direction. Right panel: comparison of computed ADs of selected NM stations during the GLE #66 employing TSY 89 (solid lines) and TSY 01 models (dashed lines).

where α is the pitch angle, σ accounts for the width of the distribution.

Details of derived spectra and pitch angle distribution (PAD) are given in Tables 2 and 3 for the application of OTSO using IGRF + TSY 89 and IGRF + TSY 01 respectively. The merit function (Equation 9), that characterized the quality of the fit, that is the residual according to Himmelblau (1972) and Dennis and Schnabel (1996) is defined as:

$$\mathcal{D} = \frac{\sqrt{\sum_{i=1}^{m}\left[\left(\frac{\Delta N_i}{N_i}\right)_{\text{mod.}} - \left(\frac{\Delta N_i}{N_i}\right)_{\text{meas.}}\right]^2}}{\sum_{i=1}^{m}\left(\frac{\Delta N_i}{N_i}\right)_{\text{meas.}}}, \tag{9}$$

Table 2
Derived Spectral and Angular Characteristics During GLE # 66 on 29 October 2003 Fitted With Modified Power-Law Rigidity Spectrum Employing Asymptotic Direction Computed With IGRF and TSY 89 Models

Integration interval UT	J_0 ($m^{-2}s^{-1}sr^{-1}$ GV^{-1})	γ	$\delta\gamma$	σ^2 (rad^2)	Ψ (degrees)	Λ (degrees)	$\mathcal{D}$(%)
21:00–21:05	6.57E4	4.81	0.35	0.9	−33.0	25.0	10.0
21:30–21:35	1.522E5	5.57	0.25	1.77	−32.0	12.0	9.9
22:00–22:05	1.352E5	5.81	0.1	3.73	−21.0	4.0	8.2
22:30–22:35	1.412E5	6.34	0.0	10.5	−40.0	25.0	8.2
23:00–23:05	1.813E5	6.51	0.0	16.0	−39.0	26.0	7.0
23:30–23:35	1.253E5	6.65	0.0	18.0	−37.0	21.0	9.7
00:00–00:05	1.33E5	6.5	0.0	21.0	−39.0	29.0	8.0
00:30–00:35	1.3E5	6.55	0.0	23.0	−18.0	8.0	10.0
01:00–01:05	1.26E5	6.6	0.0	25.0	−5.0	−2.0	8.0
01:30–01:35	1.113E5	6.7	0.0	25.0	−7.0	−10.0	12.0
02:00–02:05	9.5E4	6.87	0.0	26.0	−3.0	−25.0	15.0

Table 3
Derived Spectral and Angular Characteristics During GLE # 66 on 29 October 2003 Fitted With Modified Power-Law Rigidity Spectrum Employing Asymptotic Direction Computed With IGRF and TSY 01 Models

Integration interval UT	J_0 ($m^{-2}s^{-1}sr^{-1}$ GV^{-1})	γ	$\delta\gamma$	σ^2 (rad^2)	Ψ (degrees)	Λ (degrees)	D(%)
21:00–21:05	7.37E4	4.75	0.35	0.8	−28.0	20.0	9.0
21:30–21:35	1.73E5	5.3	0.28	1.7	−31.0	14.0	9.5
22:00–22:05	1.41E5	5.8	0.1	3.7	−24.0	18.0	8.0
22:30–22:35	1.512E5	6.1	0.0	9.0	−32.0	26.0	9.0
23:00–23:05	1.85E5	6.27	0.0	10.0	−28.0	17.0	8.0
23:30–23:35	1.31E5	6.33	0.0	10.0	−17.0	14.0	7.0
00:00–00:05	1.45E5	6.35	0.0	11.0	−14.0	10.0	5.0
00:30–00:35	1.42E5	6.4	0.0	12.0	−9.0	2.0	6.0
01:00–01:05	1.35E5	6.5	0.0	15.0	−1.0	−5.0	8.0
01:30–01:35	1.15E5	6.6	0.0	18.0	−2.0	−12.0	9.0
02:00–02:05	9.8E4	6.7	0.0	21.0	4.0	−26.0	12.0

Normally $D \leq 5\%$ for strong events (e.g. see Vashenyuk et al., 2006), whilst for weak events it is ≈10%–15%, in some cases it can even approach 20% (for details see Mishev et al., 2018, 2022).

The derived GLE spectral and PAD employing different combinations of magnetospheric models, namely IGFR + TSY 89 and IGRF + TSY 01 are comparable, despite several differences in ADs, specifically for McMurdo (MCMD) and Terre Adelie (TERA) NMs, for details see the right panel of Figure 5. Virtually the same spectra and PAD can be explained by the complexity of the unfolding procedure (see the discussion in Himmelblau (1972) and Mishev, Koldobskiy, Usoskin, et al. (2021)). In general, the employment of IGRF + TSY 01 resulted on slightly harder spectra, wider PAD and reduced D . This implies that the combination of IGRF + TSY 01 provides a more realistic model and improves the quality of the unfolding procedure. However, TSY 01 cannot be used for historical events that lack the necessary space weather data. Under these circumstances TSY 89 can be used to provide quick and satisfactory results. While TSY 89 provides acceptable results for most events, events with a Kp index above 6 should be treated with caution and latter Tsyganenko models such as TSY 96 and TSY 01 are recommended for the corresponding computations. Note, that the ADs of South Pole (SOPO), the NM with the greatest count rate increase, which is the station with maximal weight during the optimization, are in practice the same.

OTSO was also used for the analysis of GLE # 71, which occurred on 17 May 2012. The event was observed as a weak enhancement of the count rates at several NMs with greater signals recorded by APTY, OULU, and SOPO/SOPB NMs, while the other stations registered marginal count rate increases. This implied large anisotropy of the SEPs, confirmed by the following analysis (e.g., Kocharov et al., 2018; Mishev et al., 2014). Here, the angular distribution of the arriving SEPs was fitted by complicated PAD with a shape similar to that considered by Cramp et al. (1997), namely superposition of two Gaussians:

$$G(\alpha(P)) \sim \exp\left(-\alpha^2/\sigma_1^2\right) + B * \exp\left(-\left(\alpha - \alpha'\right)^2/\sigma_2^2\right) \quad (10)$$

where α is the pitch angle, σ_1 and σ_2 are parameters corresponding to the width of the PAD, B and α' are parameters corresponding to the contribution of the second Gaussian, including the direction nearly opposite to the derived axis of symmetry. The best fit for the spectra was obtained by employing modified power-law, details given in Table 4. The derived characteristics of the SEPs during GLE # 71 are in practice the same as by Mishev, Koldobskiy, Usoskin, et al. (2021), and are in good agreement with the PAMELA direct measurements (for details see Adriani et al., 2015).

4. Conclusion

A new open-source tool for conducting magnetospheric computations, called OTSO, has been developed at the request of the wider CR research community. This new tool can be downloaded from the github repository

Table 4
Derived Spectral and Angular Characteristics During GLE # 71 on 17 May 2012 Fitted With Modified Power-Law Rigidity Spectrum Employing Asymptotic Direction Computed With IGRF and TSY 89 Models

Integration interval UT	J_0[m^{-2}s^{-1}sr^{-1} GV^{-1}]	γ	$\delta\gamma$	σ_1^2(rad)	B	σ_2^2(rad)	α' (rad)	Ψ (degrees)	Λ (degrees)	N
01:50–01:55	1.28E5	−3.6	0.5	0.38	0.45	1.2	2.38	−18.0	55.0	11
02:00–02:05	2.53E5	−4.68	0.65	1.3	0.53	1.52	2.43	−21.0	62.0	8
02:15–02:20	2.39E5	−5.53	0.6	1.25	0.52	1.51	2.56	−12.0	64.0	5
02:30–02:35	1.81E5	−6.77	0.15	1.81	0.61	1.32	2.55	−10.0	57.0	6
02:45–02:50	1.43E5	−7.07	0.07	2.05	0.57	1.4	2.39	−10.0	41.2	7
03:00–03:05	1.24E5	−7.3	0.02	2.2	0.58	1. 1	2.41	−6.0	34.0	8
03:15–03:20	1.03E5	−7.6	0.0	2.4	0.58	1.3	2.41	−4.0	25.0	8
03:30–03:35	9.82E4	−7.8	0.0	3.0	0.6	2.1	2.43	−7.0	27.0	11

(https://github.com/NLarsen15/OTSO). This repository contains the source code and user manual, which details how to install and instructions on how to use OTSO. The primary aim of which is to provide a user friendly alternative to older tools that fulfill the same purpose, such as MAGNETOCOSMICS.

OTSO has a good agreement with other magnetospheric computation tools, with the variations in results being likely due to differences in the integration methods used. Further study into the impact various integration methods is planned in forthcoming work. New models, integration methods, and optimizations will be incorporated into OTSO over time by the community upon scientific goals requests. Some of the additions to OTSO will allow it to more accurately recreate older tools. The open-source and community driven element of this new tool will allow it to evolve into a robust magnetospheric computation tool that can facilitate the many needs of the CR research community, including space weather service(s), latitude surveys etc…(e.g., Mavromichalaki et al., 2018; Nuntiyakul et al., 2020). OTSO has been designed to be as user friendly as possible, for both those wishing to edit the program and those with little programming knowledge. The main tool being accessed via python opens the tool up to computer novices and the inclusion of libraries such as IRBEM provides a strong foundation for OTSO's further development. As such the new tool provides a good starting point for a community driven magnetospheric computation tool.

The creation of OTSO bolsters the CR research field's arsenal of tools that can be used to study CRs in the Earth's magnetosphere, providing the basis for detailed analysis of various CR experiments including GLEs and space weather service(s).

Within this work OTSO was successfully used for the analysis of two GLEs, namely the event that occurred during one of the strongest geomagnetic storms, GLE #66 on 29 October 2003, and the widely studied complex event, used for verification of NM data analysis using PAMELA measurements, GLE #71 that occurred on 17 May 2012. OTSO was able to obtain a good agreement with prior studies and in situ space-borne measurements for these two events, proving that it is capable of being used to study complex events, such as those with high anisotropy like GLE #71, as well as events during intense and complicated magnetospheric conditions, such as GLE #66. Hence, it has been demonstrated that OTSO can be used as a reliable tool for geomagnetospheric computations under various conditions and circumstances, providing the necessary basis for strong SEP analysis.

As such OTSO represents, a community requested new generation tool, with the possibility for constant improvement, providing reliable geomagnetospheric computations related to CR research.

Appendix A: Tool Comparison

Here we present additional data related to comparing OTSO with other similar tools. Figure A1 provides a visual comparison between the effective cutoff rigidities computed at various NMs, seen in Table 1, using OTSO and MAGNETOCOSMICS. While non-essential to the initial analysis within this work, comparing OTSO to other well-known tools besides MAGNETOCOSMICS can help to validate its use. A cursory comparison between OTSO and several of these tools is shown in Table A1. The agreement seen between OTSO and

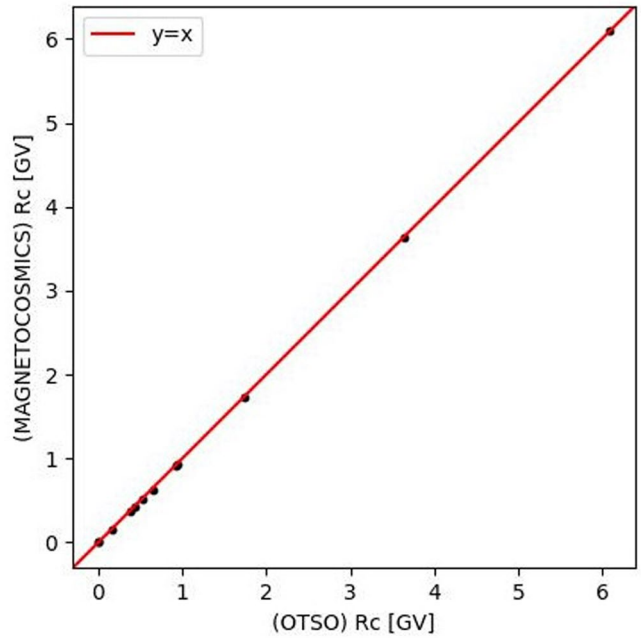

Figure A1. Visualization of the cutoff data produced by both OTSO and MAGNETOCOSMICS seen in Table 1. A simple $y = x$ dichotomous line is also plotted to emphasize the agreement between the two tools.

Table A1
Comparison of the Computed Vertical Effective Cutoff Rigidity on the Prime Meridian During the 2015 Epoch Using Four Different Geomagnetic Tools: OTSO, MAGNETOCOSMICS, D. Smart and Shea (2020), and COR (Gecášek et al., 2022)

	Vertical cutoff rigidity [GV]			
Latitude	OTSO	MAGNETOCOSMICS	Shea and Smart	COR
90	0.00	0.01	0.00	0.04
60	1.22	1.25	1.13	1.13
30	11.78	11.95	11.73	11.69
0	13.45	12.66	13.56	13.68
−30	5.37	5.38	5.53	5.26
−60	1.52	1.59	1.43	1.38
−90	0.09	0.1	0.04	0.08

Note. Only the IGRF internal magnetic field model was used during computation, no external field was used.

MAGNETOCOSMICS appears to extend to these other tools as well, however, further investigation would be required to determine if this is indeed the case.

Data Availability Statement

OTSO is available from GitHub (https://github.com/NLarsen15/OTSO) and Zenodo (https://doi.org/10.5281/zenodo.7516233) (Larsen, 2022). The fortran source of Tsyganenko models are freely available at https://geo.phys.spbu.ru/tsyganenko/empirical-models/. The NM count rate increase during GLE # 66 and GLE # 71 are available on-line at International GLE database http://gle.oulu.fi. K_p index values are provided by Space Weather Prediction Center of The National Aeronautics and Space Administration (NASA) https://www.swpc.noaa.gov/products/planetary-k-index. The ACE satellite data are retrieved from http://www.srl.caltech.edu/ACE/ASC/level2/. Data provided for the COR comparison in the appendix was obtained via the COR website https://cor.crmodels.org/homepage/data. We provide as electronic supplement the computed with OTSO

asymptotic directions used for the analysis of GLE # 66, GLE # 70, and GLE # 71 for the purposes of peer review, this data is publicly available from a Zenodo repository (https://doi.org/10.5281/zenodo.7380888) (Larsen et al., 2022). The unfolding of the NM data is performed using Levenberg-Marquardt algorithm employed in the frame of MINPACK freely available at https://netlib.org/minpack/.

Acknowledgments
This work was supported by the Academy of Finland (project 330064 QUASARE and 321882 ESPERA) and the University of Oulu Grant SARPEDON. We acknowledge NMDB and all of the colleagues and PIs from the NM stations who kindly provided the data used in this study. We also acknowledge the use of the IRBEM library (version 4.4.0), the latest version of which can be found at https://doi.org/10.5281/zenodo.6867552 . This work benefited from the SCOSTEP PRESTO steering committee grant for improvement of the records of the GLE database. The Finnish Academy of Science and Letters provided additional funding for this work via the Vilho, Yrjö and Kalle Väisälä grant. The computed asymptotic directions are provided as digital appendix. We acknowledge neutron monitor database (NMDB) and all the colleagues and PIs from the neutron monitor stations, who provided the data for the analysis of GLE # 66 and GLE #71: AATB, APTY, ATHN, BERN, BKSN, BRBG, CALG, CAPS, ERVN, FSMT, HRMS, INVK, IRKT, IRK2, IRK3, JUNG, JUN1, KERG, KIEL, KGSN, KIEL, LARC, LMKS, MCMD, MGDN, MOSC, MXCO, NAIN, NRLK, NVBK, NWRK, OULU, PTFM, PWNK, SOPO, SNAE, TERA, THUL, TSMB, TXBY, and YKTK.

References

Adriani, O., Barbarino, G., Bazilevskaya, G., Bellotti, R., Boezio, M., Bogomolov, E., et al. (2015). Pamela's measurements of magnetospheric effects on high-energy solar particles. *The Astrophysical Journal Letters*, *801*(1), L3. https://doi.org/10.1088/2041-8205/801/1/L3

Adriani, O., Barbarino, G. C., Bazilevskaya, G. A., Bellotti, R., Boezio, M., Bogomolov, E. A., et al. (2017). Ten years of PAMELA in space. *Rivista del Nuovo Cimento*, *40*(10), 473–522. https://doi.org/10.1393/ncr/i2017-10140-x

Agostinelli, S., Allison, J., Amako, K., Apostolakis, J., Araujo, H., Arce, P., et al. (2003). Geant4—A simulation toolkit. *Nuclear Instruments and Methods in Physics Research Section A: Accelerators, Spectrometers, Detectors and Associated Equipment*, *506*(3), 250–303. https://doi.org/10.1016/S0168-9002(03)01368-8

Aguilar, M., Ali Cavasonza, L., Ambrosi, G., Arruda, L., Attig, N., Barao, F., et al. (2021). The alpha magnetic spectrometer (AMS) on the international space station: Part II results from the first seven years. *Physics Reports*, *894*, 1–116. https://doi.org/10.1016/j.physrep.2020.09.003

Aleksandrov, L. (1971). The Newton-Kantorovich regularized computing processes. *USSR Computational Mathematics and Mathematical Physics*, *11*(1), 46–57. https://doi.org/10.1016/0041-5553(71)90098-X

Alken, P., Thébault, E., Beggan, C. D., Amit, H., Aubert, J., Baerenzung, J., et al. (2021). International geomagnetic reference field: The thirteenth generation. *Earth Planets and Space*, *73*(1), 49. https://doi.org/10.1186/s40623-020-01288-x

Aster, R., Borchers, B., & Thurber, C. (2005). *Parameter estimation and inverse problems*. Elsevier.

Biswas, S. (2000). *Cosmic perspectives in space physics* (Vol. 242). Springer. https://doi.org/10.1007/978-94-011-4651-7_6

Blasi, P. (2013). The origin of galactic cosmic rays. *Astronomy and Astrophysics Review*, *21*(1), 70. https://doi.org/10.1007/s00159-013-0070-7

Bütikofer, R. (2018). Cosmic ray particle transport in the Earth's magnetosphere. 79–94. https://doi.org/10.1007/978-3-319-60051-2_5

Bütikofer, R., Flückiger, E., Desorgher, L., Moser, M., & Pirard, B. (2009). The solar cosmic ray ground-level enhancements on 20 January 2005 and 13 December 2006. *Advances in Space Research*, *43*(4), 499–503. https://doi.org/10.1016/j.asr.2008.08.001

Clem, J., Bieber, J. W., Evenson, P., Hall, D., Humble, J. E., & Duldig, M. (1997). Contribution of obliquely incident particles to neutron monitor counting rate. *Journal of Geophysical Research*, *102*(A12), 919–26926. https://doi.org/10.1029/97ja02366

Cooke, D., Humble, J., Shea, M., Smart, D., Lund, N., Rasmussen, I., et al. (1991). On cosmic-ray cutoff terminology. *Il Nuovo Cimento C*, *14*(3), 213–234. https://doi.org/10.1007/bf02509357

Costa, R., Jr., & Leigui de Oliveira, M. (2019). Analysis of the performance of numerical integration methods for the tracking of ultra-high energy cosmic rays. *Journal of Computational Physics*, *392*, 432–443. https://doi.org/10.1016/j.jcp.2019.04.058

Cramp, J., Duldig, M., Flückiger, E., Humble, J., Shea, M., & Smart, D. (1997). The October 22, 1989, solar cosmic enhancement: Ray an analysis the anisotropy spectral characteristics. *Journal of Geophysical Research*, *102*(A11), 24237–24248. https://doi.org/10.1029/97ja01947

Cramp, J., Humble, J., & Duldig, M. (1995). The cosmic ray ground-level enhancement of 24 October 1989. In *Proceedings Astronomical Society of Australia* (Vol. 11, pp. 28–32).

Dennis, J., & Schnabel, R. (1996). *Numerical methods for unconstrained optimization and nonlinear equations*. Prentice-Hall.

Desai, M., & Giacalone, J. (2016). Large gradual solar energetic particle events. *Living Reviews in Solar Physics*, *13*(1), 3. https://doi.org/10.1007/s41116-016-0002-5

Desorgher, L. (2006). Magnetocosmics users manual [Computer Software Manual]. Retrieved from http://cosray.unibe.ch//%7Elaurent/planetocosmics/

Flückiger, E. O., & Kobel, E. (1990). Aspects of combining models of the Earth's internal and external magnetic field. *Journal of Geomagnetism and Geoelectricity*, *42*(9), 1123–1136. https://doi.org/10.5636/jgg.42.1123

Forbush, S. (1937). On the effects in cosmic-ray intensity observed during the recent magnetic storm. *Physical Review*, *51*(12), 1108–1109. https://doi.org/10.1103/physrev.51.1108.3

Formisano, V., Domingo, V., & Wenzel, K.-P. (1979). The three-dimensional shape of the magnetopause. *Planetary and Space Science*, *27*(9), 1137–1149. https://doi.org/10.1016/0032-0633(79)90134-X

Gaisser, T. K., Engel, R., & Resconi, E. (2016). Cosmic rays. In *Cosmic rays and particle physics* (2nd ed., pp. 1–11). Cambridge University Press. https://doi.org/10.1017/CBO9781139192194.003

Gecášek, D., Bobík, P., Genči, J., Villim, J., & Vaško, M. (2022). COR system: A tool to evaluate cosmic ray trajectories in the Earth's magnetosphere. *Advances in Space Research*, *70*(4), 1153–1168. https://doi.org/10.1016/j.asr.2022.06.001

Gerontidou, M., Katzourakis, N., Mavromichalaki, H., Yanke, V., & Eroshenko, E. (2021). World grid of cosmic ray vertical cut-off rigidity for the last decade. *Advances in Space Research*, *67*(7), 2231–2240. https://doi.org/10.1016/j.asr.2021.01.011

Golub, G., Hansen, P., & O'Leary, D. P. (1999). Tikhonov regularization and total least squares. *SIAM Journal on Matrix Analysis and Applications*, *21*(1), 185–194. https://doi.org/10.1137/s0895479897326432

Gopalswamy, N., Barbieri, L., Cliver, E., Lu, G., Plunkett, S., & Skoug, R. (2005). Introduction to violent Sun-Earth connection events of October-November 2003. *Journal of Geophysical Research*, *110*(A9), A09S00. https://doi.org/10.1029/2005JA011268

Gopalswamy, N., Xie, H., Yashiro, S., Akiyama, S., Mäkelä, P., & Usoskin, I. (2012). Properties of ground level enhancement events and the associated solar eruptions during solar cycle 23. *Space Science Reviews*, *171*(1–4), 23–60. https://doi.org/10.1007/s11214-012-9890-4

Grieder, P. (2001). *Cosmic rays at Earth researcher's reference manual and data book*. Elsevier Science.

Himmelblau, D. (1972). *Applied nonlinear programming*. Mcgraw-Hill(Tx).

Jordan, C. E. (1994). Empirical models of the magnetospheric magnetic field. *Reviews of Geophysics*, *32*(2), 139–157. https://doi.org/10.1029/94RG00100

Kobel, E. (1992). Zu den magnetosphärischen effekten der kosmischen strahlung. (Inaugural Dissertation). University of Bern.

Kocharov, L., Pohjolainen, S., Reiner, M., Mishev, A., Wang, H., Usoskin, I., & Vainio, R. (2018). Spatial organization of seven extreme solar energetic particle events. *The Astrophysical Journal Letters*, *862*(2), L20. https://doi.org/10.3847/2041-8213/aad18d

Koldobskiy, S., Kovaltsov, G., Mishev, A., & Usoskin, I. (2019). New method of assessment of the integral fluence of solar energetic (>1 GV rigidity) particles from neutron monitor data. *Solar Physics*, *294*(7), 94. https://doi.org/10.1007/s11207-019-1485-8

Koldobskiy, S., Raukunen, O., Vainio, R., Kovaltsov, G., & Usoskin, I. (2021). New reconstruction of event-integrated spectra (spectral fluences) for major solar energetic particle events. *Astronomy and Astrophysics*, *647*, A132. https://doi.org/10.1051/0004-6361/202040058

Kudela, K., Bučik, R., & Bobik, P. (2008). On transmissivity of low energy cosmic rays in disturbed magnetosphere. *Advances in Space Research*, *42*(7), 1300–1306. https://doi.org/10.1016/j.asr.2007.09.033

Kudela, K., & Usoskin, I. (2004). On magnetospheric transmissivity of cosmic rays. *Czechoslovak Journal of Physics*, *54*(2), 239–254. https://doi.org/10.1023/b:cjop.0000014405.61950.e5

Larsen, N. (2022). *Nlarsen15/OTSO: OTSO*. Zenodo. https://doi.org/10.5281/zenodo.7516233

Larsen, N., Mishev, A., & Usoskin, I. (2022). *A new open-source geomagnetosphere propagation tool (OTSO) and its applications—Data*. Zenodo. https://doi.org/10.5281/zenodo.7380888

Levenberg, K. (1944). A method for the solution of certain non-linear problems in least squares. *Quarterly of Applied Mathematics*, *2*, 164–168. https://doi.org/10.1090/qam/10666

Lin, R. L., Zhang, X. X., Liu, S. Q., Wang, Y. L., & Gong, J. C. (2010). A three-dimensional asymmetric magnetopause model. *Journal of Geophysical Research*, *115*(A4), A04207. https://doi.org/10.1029/2009JA014235

Liu, Y., & Hayashi, K. (2006). The 2003 October-November fast halo coronal mass ejections and the large-scale magnetic field structures. *The Astrophysical Journal*, *640*(2 I), 1135–1141. https://doi.org/10.1086/500290

Marquardt, D. (1963). An algorithm for least-squares estimation of nonlinear parameters. *SIAM Journal on Applied Mathematics*, *11*(2), 431–441. https://doi.org/10.1137/0111030

Mavrodiev, S., Mishev, A., & Stamenov, J. (2004). A method for energy estimation and mass composition determination of primary cosmic rays at the Chacaltaya observation level based on the atmospheric Cherenkov light technique. *Nuclear Instruments and Methods in Physics Research Section A: Accelerators, Spectrometers, Detectors and Associated Equipment*, *530*(3), 359–366. https://doi.org/10.1016/j.nima.2004.04.226

Mavromichalaki, H., Gerontidou, M., Paschalis, P., Paouris, E., Tezari, A., Sgouropoulos, C., et al. (2018). Real-time detection of the ground level enhancement on 10 September 2017 by A.Ne.Mo.S.: System report. *Space Weather*, *16*(11), 1797–1805. https://doi.org/10.1029/2018SW001992

Mavromichalaki, H., Papaioannou, A., Plainaki, C., Sarlanis, C., Souvatzoglou, G., Gerontidou, M., et al. (2011). Applications and usage of the real-time neutron monitor database. *Advances in Space Research*, *47*(12), 2210–2222. https://doi.org/10.1016/j.asr.2010.02.019

Mishev, A., Kocharov, L., Koldobskiy, S., Larsen, N., Riihonen, E., Vainio, R., & Usoskin, I. (2022). High-resolution spectral and anisotropy characteristics of solar protons during the GLE N°73 on 28 October 2021 derived with neutron-monitor data analysis. *Solar Physics*, *297*(7), 88. https://doi.org/10.1007/s11207-022-02026-0

Mishev, A., Kocharov, L., & Usoskin, I. (2014). Analysis of the ground level enhancement on 17 may 2012 using data from the global neutron monitor network. *Journal of Geophysical Research: Space Physics*, *119*(2), 670–679. https://doi.org/10.1002/2013ja019253

Mishev, A., Koldobskiy, S., Kocharov, L., & Usoskin, I. (2021a). GLE # 67 event on 2 November 2003: An analysis of the spectral and anisotropy characteristics using verified yield function and detrended neutron monitor data. *Solar Physics*, *296*(5), 79. https://doi.org/10.1007/s11207-021-01832-2

Mishev, A., Koldobskiy, S., Usoskin, I., Kocharov, L., & Kovaltsov, G. (2021b). Application of the verified neutron monitor yield function for an extended analysis of the GLE # 71 on 17 may 2012. *Space Weather*, *19*(2), e2020SW002626. https://doi.org/10.1029/2020SW002626

Mishev, A., Poluianov, S., & Usoskin, S. (2017). Assessment of spectral and angular characteristics of sub-GLE events using the global neutron monitor network. *Journal of Space Weather and Space Climate*, *7*, A28. https://doi.org/10.1051/swsc/2017026

Mishev, A., & Usoskin, I. (2016). Analysis of the ground level enhancements on 14 July 2000 and on 13 December 2006 using neutron monitor data. *Solar Physics*, *291*(4), 1225–1239. https://doi.org/10.1007/s11207-016-0877-2

Mishev, A., Usoskin, I., Raukunen, O., Paassilta, M., Valtonen, E., Kocharov, L., & Vainio, R. (2018). First analysis of GLE 72 event on 10 September 2017: Spectral and anisotropy characteristics. *Solar Physics*, *293*, 136. https://doi.org/10.1007/s11207-018-1354-x

Moraal, H., & McCracken, K. (2012). The time structure of ground level enhancements in solar cycle 23. *Space Science Reviews*, *171*(1–4), 85–95. https://doi.org/10.1007/s11214-011-9742-7

Nevalainen, J., Usoskin, I., & Mishev, A. (2013). Eccentric dipole approximation of the geomagnetic field: Application to cosmic ray computations. *Advances in Space Research*, *52*(1), 22–29. https://doi.org/10.1016/j.asr.2013.02.020

Nuntiyakul, W., Mangeard, P.-S., Ruffolo, D., Evenson, P., Bieber, J., Clem, J., et al. (2020). Direct determination of a bare neutron counter yield function. *Journal of Geophysical Research: Space Physics*, *125*(4), e2019JA027304. https://doi.org/10.1029/2019JA027304

Rao, U. R., McCracken, K. G., & Venkatesan, D. (1963). Asymptotic cones of acceptance and their use in the study of the daily variation of cosmic radiation. *Journal of Geophysical Research (1896-1977)*, *68*(2), 345–369. https://doi.org/10.1029/JZ068i002p00345

Shea, M., & Smart, D. (1982). Possible evidence for a rigidity-dependent release of relativistic protons from the solar corona. *Space Science Reviews*, *32*(1–2), 251–271. https://doi.org/10.1007/bf00225188

Shea, M., & Smart, D. (2012). Space weather and the ground-level solar proton events of the 23rd solar cycle. *Space Science Reviews*, *171*(1–4), 161–188. https://doi.org/10.1007/s11214-012-9923-z

Shue, J.-H., Song, P., Russell, C. T., Steinberg, J. T., Chao, J. K., Zastenker, G., et al. (1998). Magnetopause location under extreme solar wind conditions. *Journal of Geophysical Research*, *103*(A8), 17691–17700. https://doi.org/10.1029/98JA01103

Sibeck, D. G., Lopez, R. E., & Roelof, E. C. (1991). Solar wind control of the magnetopause shape, location, and motion. *Journal of Geophysical Research*, *96*(A4), 5489–5495. https://doi.org/10.1029/90ja02464

Simpson, J. (2000). The cosmic ray nucleonic component: The invention and scientific uses of the neutron monitor. *Space Science Reviews*, *93*(1/2), 11–32. https://doi.org/10.1023/A:1026567706183

Smart, D. F., & Shea, M. (2001). *Geomagnetic cutoff rigidity computer program: Theory, software description and example*. NASA STI/Recon Technical Report N.

Smart, D., & Shea, M. (2020). Vertical geomagnetic cutoff rigidities for epoch 2015. In *36th International Cosmic Ray Conference (ICRC2019)* (p. 1154). https://doi.org/10.22323/1.358.1154

Smart, D. F., Shea, M., & Flückiger, E. (2000). Magnetospheric models and trajectory computations. *Space Science Reviews*, *93*(1), 305–333. https://doi.org/10.1023/a:1026556831199

Smart, D. F., & Shea, M. A. (1981). Optimum step length control for cosmic-ray trajectory calculations. In *International cosmic ray conference* (Vol. 4, p. 208).

Tikhonov, A., Goncharsky, A., Stepanov, V., & Yagola, A. (1995). *Numerical methods for solving ill-posed problems*. Kluwer Academic Publishers.

Tsyganenko, N. A. (1987). Global quantitative models of the geomagnetic field in the cislunar magnetosphere for different disturbance levels. *Planetary and Space Science*, *35*(11), 1347–1358. https://doi.org/10.1016/0032-0633(87)90046-8

Tsyganenko, N. A. (1989). A magnetospheric magnetic field model with a warped tail current sheet. *Planetary and Space Science*, *37*(1), 5–20. https://doi.org/10.1016/0032-0633(89)90066-4

Tsyganenko, N. A. (2002). A model of the near magnetosphere with a dawn-dusk asymmetry. *Journal of Geophysical Research*, *107*(A8), SMP12-1–SMP12-15. https://doi.org/10.1029/2001JA000219

Tsyganenko, N. A., Singer, H., & Kasper, J. (2003). Storm-time distortion of the inner magnetosphere: How severe can it get. *Journal of Geophysical Research*, *108*(A5), 1209. https://doi.org/10.1029/2002JA009808

Tsyganenko, N. A. (1995). Modeling the Earth's magnetospheric magnetic field confined within a realistic magnetopause. *Journal of Geophysical Research*, *100*(A4), 5599–5612. https://doi.org/10.1029/94JA03193

Tsyganenko, N. A. (1996). Effects of the solar wind conditions on the global magnetospheric configuration as deduced from data-based field models.

Tsyganenko, N. A. (2002a). A model of the near magnetosphere with a dawn-dusk asymmetry 1. Mathematical structure. *Journal of Geophysical Research*, *107*(A8), SMP12-1–SMP12-15. https://doi.org/10.1029/2001JA000219

Tsyganenko, N. A. (2002b). A model of the near magnetosphere with a dawn-dusk asymmetry 2. Parameterization and fitting to observations. *Journal of Geophysical Research*, *107*(A8), SMP10-1–SMP10-17. https://doi.org/10.1029/2001JA000220

Vashenyuk, E., Balabin, Y., Gvozdevsky, B., & Schur, L. (2008). Characteristics of relativistic solar cosmic rays during the event of December 13, 2006. *Geomagnetism and Aeronomy*, *48*(2), 149–153. https://doi.org/10.1134/s0016793208020035

Vashenyuk, E., Balabin, Y., Perez-Peraza, J., Gallegos-Cruz, A., & Miroshnichenko, L. (2006). Some features of the sources of relativistic particles at the sun in the solar cycles 21-23. *Advances in Space Research*, *38*(3), 411–417. https://doi.org/10.1016/j.asr.2005.05.012